Received: 25 April 2021 | Revised: 3 August 2022 | Accepted: 5 August 2022

DOI: 10.1002/stc.3077

RESEARCH ARTICLE

WILEY

A new open-database benchmark structure for vibration-based Structural Health Monitoring

Stefan Wernitz | **Benedikt Hofmeister** | **Clemens Jonscher** | **Tanja Grießmann** | **Raimund Rolfes**

Institute of Structural Analysis, Leibniz University Hannover, Hannover, Germany

Correspondence
Stefan Wernitz, Institute of Structural Analysis, Leibniz University Hannover, Hannover, Lower Saxony, Germany.
Email: s.wernitz@isd.uni-hannover.de

Funding information
Bundesministerium für Wirtschaft und Energie; Deutsche Forschungsgemeinschaft, Grant/Award Number: SFB 1463; Federal Ministry of Economic Affairs and Energy of the Federal Republic of Germany, Grant/Award Number: FKZ 0325936I

Abstract

Vibration-based Structural Health Monitoring is an ongoing field of research in many engineering disciplines. As for civil engineering, plenty of experimental structures have been erected in the past decades, both under laboratory and real-life conditions. Some of these facilities became a benchmark for different kinds of methods associated with Structural Health Monitoring such as damage analysis and Operational Modal Analysis, which led to fruitful developments in the global research community. When it comes to the continuous monitoring and assessment of the structural integrity of mechanical systems exposed to environmental and operational variability, the robustness and adaptability of the applied methods is of utmost importance. Such properties cannot be fully evaluated under laboratory conditions, which highlights the necessity of outdoor measurement campaigns. To this end, we introduce a test facility for Structural Health Monitoring comprising a lattice tower exposed to realistic conditions and featuring multiple reversible damage mechanisms. The structure located near Hanover in Northern Germany is densely equipped with sensors to capture the structural dynamics. The environmental conditions are monitored in parallel. The obtained continuous measurement data can be accessed online in an open repository. That is the foundation for benchmarks, consisting of a growing data set that enables the development, evaluation, and comparison of Structural Health Monitoring strategies and methods. In this article, we offer a documentation of the test facility and the data acquisition system. Lastly, we characterize the structural dynamics with the help of a finite element model and by analyzing several month of data.

KEYWORDS

modal analysis, open-access database, outdoor benchmark structure, reversible damages, Structural Health Monitoring

1 | INTRODUCTION

In the past three decades, Structural Health Monitoring (SHM) evolved to an intensively studied field of research, as it promises to replace classical time- and cost-consuming human inspections of engineering structures with an effective continuous surveillance strategy. The fundamental idea is to infer the structural integrity of a mechanical system based on changes in the vibration characteristics,[1] whereas the main aspects of research arise directly from the workflow of SHM[2] and the paradigm of handling information.[3,4] In the last 30 years, great effort has been put into the development of damage-sensitive features, the field of system identification and Operational Modal Analysis (OMA), the handling of environmental and operational variations (EOVs), and the recognition of abnormalities.[5]

With increasing interest and the extension of application fields, the need for benchmark structures arises. The purpose is not necessarily to create a basis for the comparison of methods, but also for implementation and validation of novel strategies in the context of SHM such as system identification and damage analysis, as the conduction and maintenance of experiments requires experience and high effort. Laboratory tests are readily used, as they can be designed in such a way that their dynamics are simple or feature certain characteristics. Most importantly, they are usually conducted in a controlled environment, where only a few uncertainties exist, or no varying effects through environmental and operational conditions (EOCs) need to be considered. In the sense of open research, data sets of laboratory campaigns have been published and exploited for several SHM problems. Good examples are vibration test campaigns of bookshelf structures[6,7] that feature different damages and undergo several controlled variations. The research conducted with these data sets reaches from system identification[8] to detection, localization,[9] and quantification[10] of damage, to name but a few applications. In civil engineering, where the structures are particularly large, complex, and/or voluminous laboratory systems are of interest. By that, more realistic benchmark objects become relevant, which feature dynamic and constructional properties that are closer to the practical application. Motivated by that, large shear-building-like benchmark structures and problems were designed.[11–13] Further, wind turbines have drawn increasing interest in the research for SHM of civil engineering structures[14] because of their extensive and remote installations, and their complex and varying dynamical properties. In particular, the focus lies on the monitoring of rotor blades[15–18] and foundations,[19] as these members are prone to damages. Regarding the former, an open-database benchmark structure was implemented by Ou et al,[20] which features several damage positions and intensities. The benchmark structure, a miniature rotor blade with a length of 1.75 m, was exposed to varying temperatures in a climate chamber to enable the damage detection under varying environmental conditions.

Naturally, laboratory tests provide a controlled environment for the research and testing of specific phenomena and methods. However, to test the robustness of certain schemes, more practical scenarios, which hold a larger potential for uncertainty and variability, should be considered. Another challenge is that the ambient excitation, which is the major excitation source for many civil engineering structures like bridges and towers, can hardly be simulated in a laboratory setup. To this end, large testing campaigns have been conducted in the past. The provided measurements have been suitable for many researchers all over the world as a basis for the development and comparison of all kinds of SHM methods. By that, these structures became de-facto benchmark objects. Early examples for such large-scale tests are the studies associated with the I40 and Alamosa Canyon bridges conducted by Farrar et al.[21] In the context of SHM of bridges, probably the most popular benchmark structure is the Z24 bridge.[22,23] Unlike the I40 and Alamosa Canyon bridge, structural damages were introduced there. Because of a nonlinear temperature dependence and the monitoring period of almost a year, the Z24 bridge led to fruitful developments in the context of damage identification under varying EOCs.[24–28] Beside other research, plenty of contributions toward the application and comparison of system identification and OMA techniques were made.[29–31] Recently, short measurement campaigns were conducted at the S101 bridge including the acquisition of data under healthy and progressively damaged conditions.[32] The bridge was finally demolished, similar to the Z24 bridge. This benchmark object inspired relevant research in the field of vibration-based damage detection[33–35] and localization[36] as well. Finally, an impressive benchmark database was presented,[37] which relates to the monitoring system of a 510-m-long cable-stayed bridge. This structure was subjected to research in the field of SHM in, for example, Huang et al.[38]

Obviously, real-life benchmark structures represent a valuable basis for the research regarding all aspects of SHM. Because of their complexity, realistic excitation, and therefore, their inherent sources of uncertainty, they help to judge whether the developed methods are ready for practical applications. Unfortunately, genuine structures that are monitored over a long period and feature at least one damage state such as the Z24 bridge are rare. Even in this case, signals were saturated,[39] which represents a loss of information, and reduces the suitability for further research regarding time-domain approaches, for instance.

In conclusion, from a scientific perspective, benchmark objects are desirable, which (i) are exposed to natural sources of excitation and variations, (ii) feature a reasonable degree of complexity, (iii) exhibit damages during their life-time in multiple intensities and at more than one position, and (iv) are measured over long periods. To fill this gap, we designed and implemented the **L**eibniz **U**niversity Test Structure for **MO**nitoring (LUMO), a lattice mast structure with a height of approximately 9 m comprising 18 reversible damages on six levels. The system is set up outdoors and is equipped with accelerometers, strain gauges, and a temperature sensor, and monitored continuously. A meteorological measurement mast located in close proximity (approximately 20 m) provides a comprehensive overview of the environmental conditions. All acquired data as well as a nominal finite element model are provided online in an open-access repository. Thereby, a benchmark object is created that enables the testing and validation of all kinds of vibration-based SHM methods for practical application.

With the present article, we introduce this new test structure to the research community and provide a detailed documentation and characterization of the dynamic properties. First, we describe the facility including the design, sensor layout, data acquisition system, and the provided data, as well as the reversible damage mechanisms. Then, a finite element model of the structure is introduced that can be utilized for numerical studies or model-based methods. In the final section, we characterize the dynamic properties of the test structure by analyzing five months of data.

2 | A TESTING FACILITY FOR SHM

The testing facility is situated on a field, 20 km south of Hanover (Lower Saxony, Germany). It comprises a steel lattice mast mounted on a concrete block foundation and a data acquisition system. In order to test multiple damage scenarios, the mast features reversible damage mechanisms on six levels along its height. The block foundation was built in October 2019, the tower was erected in June 2020, and the continuous measurements started in August 2020. In the following, we will describe the testing facility thoroughly. Starting with a general characterization, we will continue by describing the damage features and the environmental conditions. We will close this section by presenting the measurement setup, the data acquisition system, and provide details on the access to the data.

2.1 | General description of the structure

The steel lattice mast consists of three identical segments with a length of 3 m each, resulting in a total height of 9 m. The overall weight without sensors is approximately 90 kg. Each segment has three tubular legs forming a cross-section similar to an isosceles triangle and consists of seven bracing levels as well as short connecting sections at the ends. The sections end in an elliptical flange, which allows the connection of the segments in arbitrary order employing regular M10 steel bolts. A photograph of the lattice mast can be found in Figure 1.

The test structure is mounted on a concrete block foundation with the dimensions 1.5 m $\times$ 1.5 m $\times$ 0.8 m, which is embedded in cohesive soil. Therefore, an anchor plate, with eight head bolts attached to it, was integrated during the manufacturing of the foundation. To safely erect and modify the mast, the anchor plate was designed as a hinge consisting of two metal plates with a thickness of 30 mm each. The latter is kept shut by 12 M12 bolts during monitoring measurements to provide a rigid fixture of the mast. A photograph of the foundation and connector plate is given in Figure 2.

2.2 | Reversible damage features and environmental conditions

The key features of the test structure are local reversible damages that manifest themselves as stiffness and possibly mass alterations. For this purpose, on six levels of the structure, which are depicted in Figure 1, reversible damage mechanisms enable the disconnection of individual bracings. At each possible damage level, all three bracings were equipped with the damage mechanism, resulting in 18 different positions for the introduction of localized stiffness alterations. The damage features consist of two screw sockets, one with a left-hand and one with a right-hand thread, and a connection piece (threaded M10 rod). An exemplary photograph depicting damage mechanisms at damage level 6 is given in Figure 2. The damage mechanisms are activated by loosening the screw sockets and possibly removing the connection pieces resulting in a complete severance of the corresponding bracings. When damage mechanisms are

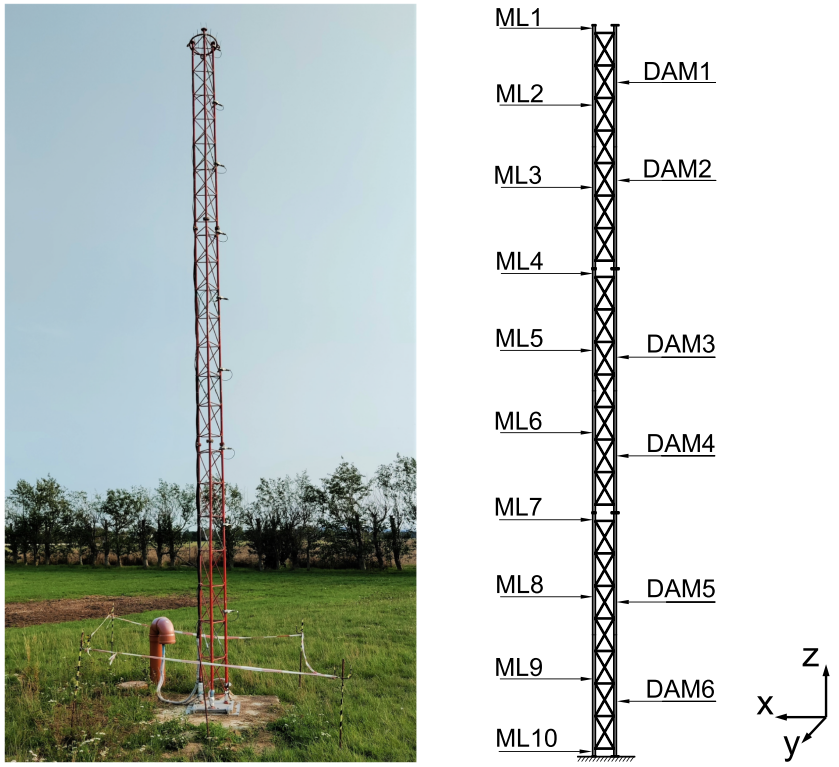

FIGURE 1 Photograph of the test structure (left), and schematic drawing including the measurement levels (MLs) and the damage locations (DAM) (right)

FIGURE 2 Photograph of the foundation and anchor plate (left), and photograph of the first bay and damage mechanism in place (right)

completely removed (screw sockets and connection piece), as was done for the currently available data of the damaged structure, the stiffness alteration comes together with a decrease of mass by approximately 155 g per damage mechanism.

As the structure is located outside, the main excitation source constitutes aerodynamic forces exerted by the wind, which mainly blows from west to south. Further, variations of the structural dynamic behavior are mainly caused by daily and seasonal temperature cycles. During visual inspections, we also recognized that the mast is occasionally sought by birds as a place to rest.

2.3 | Sensor equipment

The structure is equipped with 18 uniaxial accelerometers, three strain sensors, and one temperature sensor. They are distributed across ten horizontal measurement levels, which are schematically displayed in Figure 1. Further, a list of all measurement levels and the associated sensors and channel names together with the height of installation is given in Table 1.

MEAS 8811LF-01-005 piezoelectric accelerometers with IEPE current supply (channel names starting with *accel*) are mounted in pairs using 90° mounting brackets to measure in orthogonal deflection directions, and to capture the spatial motion in the horizontal plane. There are no acceleration sensors in the vertical direction (z axis) because of their low relevance for beam-like structures. The positioning and orientation of the accelerometers is schematically depicted in Figure 3.

Two HBM quarter-bridge strain gauges in a half-bridge setup (channel names starting with *strain*) are installed at the base at each leg (ML10) to effectively measure the axial strain close to the foundation. The strain gauges are electrically wired so that shear strains in the legs cancel out. The identifier for each leg, which is part of the channel name of each strain sensor, can be found in circled numbers in Figure 3 as well.

One Pt100 type thermocouple is mounted at the same measurement level as the strain sensors and provides the reference material temperature.

TABLE 1 Measurement levels (MLs) with associated channels and z coordinates

ML	ML1	ML2	ML3	ML4	ML5	ML6	ML7	ML8	ML9	ML10
Channel names	accel01x	...02x	...03x	...04x	...05x	...06x	...07x	...08x	...09x	strain01
										strain02
	accel01y	...02y	...03y	...04y	...05y	...06y	...07y	...08y	...09y	strain03
										temp01
Height (z in m)	8.95	8.00	7.00	5.95	5.00	4.00	2.95	2.00	1.00	0.15

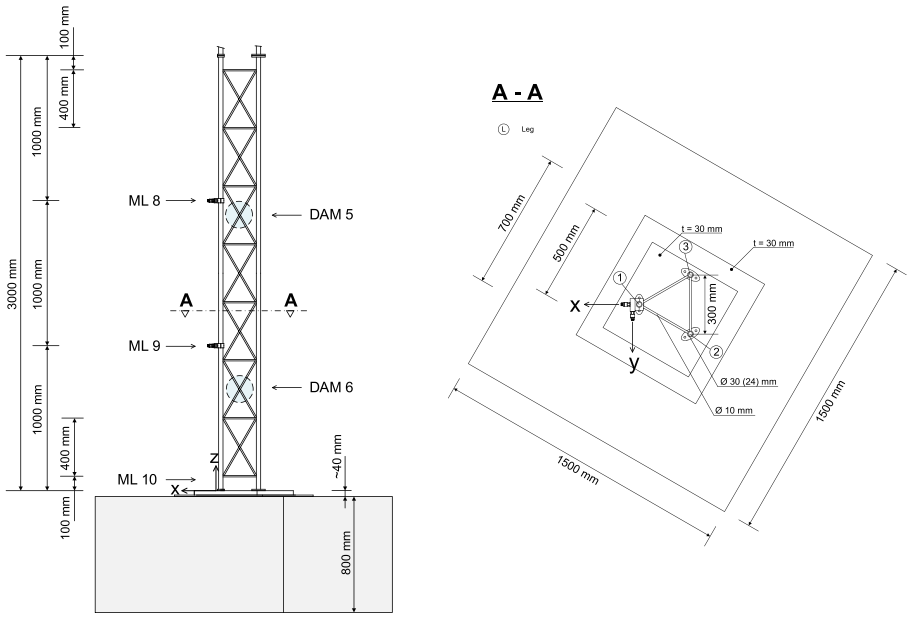

FIGURE 3 Front view of lower segment (left), and cross section with measurement directions of accelerometers (right)

2.4 | Data acquisition and supply

The data acquisition system consists of a National Instruments NI-cDAQ-9189 device connected to a host computer, both protected from the environment in a shack approximately 40 m away from the test structure. The chassis contains five NI-9234 modules for the measurements of the accelerometers, one NI-9237 module for the strain gauges, and one NI-9291 module for the temperature sensor. The data are acquired continuously at a sampling rate of 1651.61 Hz and locally stored as data blocks of 10 min on the hard drive of the host computer.

A meteorology mast erected by the Institute of Meteorology and Climatology (IMUK) of Leibniz University Hannover is positioned 20 m away from the test structure. There, the meteorological data are measured and saved as 1-min mean values. This information precisely describes the predominant environmental conditions. The information made available and their physical units are summarized in Table 2.

Here, 0° for the direction of wind refers to the northern direction, whereas 90° corresponds to the east. It should be noted that the wind measurements were initially acquired using a cup anemometer. Due to a breakdown, this device was replaced by an ultrasonic anemometer on June 21, 2021.

Measurement data from August until the end of July 2021, including all data used in this document, as well as a comprehensive documentation are uploaded to a repository of Leibniz University Hannover and can be reached through the following link:

https://data.uni-hannover.de/dataset/lumo

or

https://doi.org/10.25835/0027803

The data are available in Matlab (mat.) files and is divided in structural (acceleration, strains, and material temperature), and meteorological measurements. The former comprises 10-min data chunks organized in folders for every month. Because of the huge amount of data, each monthly folder is wrapped in zip-archives split in approximately 30 subfiles. Since no compression was conducted, these subfiles can be unpacked separately if only a portion of the monthly data is desired. To enable a targeted filtering and selection of the data, we provide metafiles for each month containing the statistical information mean, median, and variance, and information regarding the damage state of the structure for every 10-min data file.

The meteorological data (cf. Table 2) are originally owned and presented by IMUK.[40] Nevertheless, for the purpose of this research infrastructure, we provide these data together with the structural measurements under the link above, and consequently, it is organized similarly. However, for legal reasons, the associated files can only be accessed via password. We readily provide the key to the meteorological data section to every researcher from an educational institution via e-mail. Therefore, the contact information is given under the link above.

Currently, the database comprises data measured using the healthy structure as well as six damage cases that manifest themselves in two different extents of damage at three different positions, as summarized in Table 3. The database will be extended regularly comprising different damage combinations and environmental conditions to enable the research in the field of SHM. Therefore, a schedule for future measurement campaigns was added to the documentation available under the link above. This file will be updated regularly. The authors offer their support and assistance for the handling of the data and are open to suggestions regarding different types of experiments. We gladly receive e-mails addressed to the corresponding author or public.data@isd.uni-hannover.de.

TABLE 2 Available meteorological data as 1-min mean values with units and associated abbreviations

Meteorological data	Unit	Abbreviation
Air temperature (2 m above ground)	°C	AT
Relative humidity (2 m above ground)	%	RH
Sum of precipitation	mm	P
Global radiation	$W\ m\ s^{-2}$	GR
Average wind speed (10 m above ground)	$\sim s^{-1}$	AW
Max. wind speed (10 m above ground; not averaged)	$\sim s^{-1}$	MW
Direction of wind	°	WD

2.5 | Description of surrounding area

As mentioned at the beginning of Section 2, the girder mast is located on a field near the city of Hanover, Germany. The coordinates for the exact position read 52°14′35.2”N 9°48′47.1”E. For elaborate numerical analyses and the interpretation of identification results, the characterization of the wind field is beneficial. However, measuring the wind field and turbulence exceeds the scope of the presented long-term experiment and sensor setup. In order to characterize the wind conditions, additional information describing the area surrounding the test structure are given in the following.

Figure 4 depicts an overview of the field on which the girder mast is positioned. The latter is highlighted with a red dot. Moreover, the directions of measurements are given therein. The girder mast is mainly surrounded by flat farmland, though, a few objects are located nearby that might cause turbulent airflow. To assess the likelihood of occurrence, a histogram of the wind direction measurements for October 2020 is provided in Figure 4 as well. Therein, it can be seen that in most cases the wind comes from the south and south-west.

Given the common wind direction, turbulence might be caused frequently because of the hedge located south of the girder mast. However, since the hedge features a height of approximately 4-m, laminar airflow is widely expected. Other objects that might affect the aeroelastic behavior are manifested by wind turbines and trees located in the west, containers (approximately 2.5 m high) in the north, and a garden dump (height $\leq$ 3 m) located in the east of the girder mast, but again, turbulence caused by these objects are rather unlikely, as they are not within the main wind direction.

TABLE 3 Currently accessible data according to structural state and damage position (effective November 2021)

Period of data acquisition	Structural state	Damage position
Aug. 1, 2020 to Oct. 13, 2020	healthy	–
Oct. 13, 2020 to Oct. 27, 2020	damaged	damage level 6 (all damage mechanisms removed)
Oct. 27, 2020 to Nov. 9, 2020	healthy	–
Nov. 9, 2020 to Nov. 24, 2020	damaged	damage level 4 (all damage mechanisms removed)
Nov. 24, 2020 to Mar. 18, 2021	healthy	–
Mar. 18, 2021 to Apr. 20, 2021	damaged	damage level 3 (all damage mechanisms removed)
Apr. 20, 2021 to May 4, 2021	healthy	–
May 4, 2021 to May 19, 2021	damaged	damage level 6 (one damage mechanisms removed)
May 19, 2021 to May 28, 2021	healthy	–
May 28, 2021 to Jun. 14, 2021	damaged	damage level 4 (one damage mechanisms removed)
Jun. 14, 2021 to Jun. 25, 2021	healthy	–
Jun. 25, 2021 to Jul. 12, 2021	damaged	damage level 3 (one damage mechanisms removed)
Jul. 12, 2021 to Jul. 31, 2021	healthy	–

Note: For more details, see documentation and meta files within the data repository.

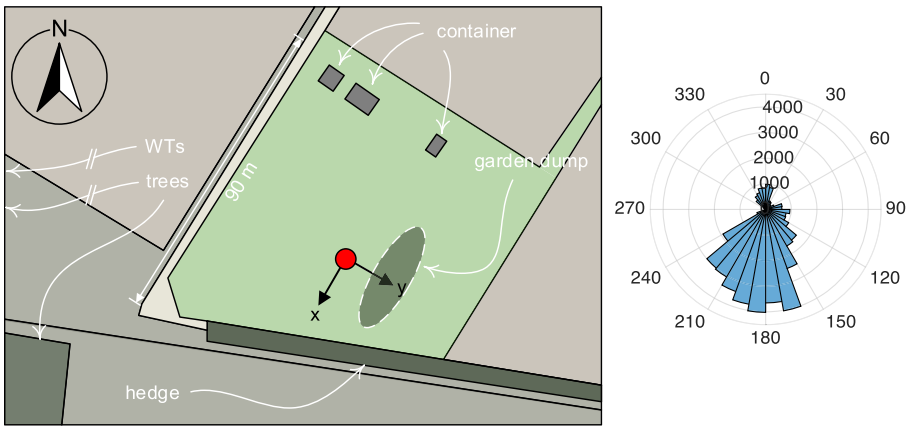

FIGURE 4 Overview of **L**eibniz **U**niversity Test Structure for **MO**nitoring's (LUMO's) (red dot) surrounding area with directions of measurement (left). Histogram of wind direction measurements for October 2020 using a bin size of 10° (right)

2.6 | Finite element calculations

The structure was modeled using finite elements to gain an insight into the structural dynamic behavior. This provides a basis for comparison, which can be used to verify the subsequent data-driven modal analysis.

Beam elements with linear interpolation were used and the structure was discretized using elements with a length of roughly 3 cm for both legs and braces. The welded connections of the braces to the legs as well as the flange connections between the segments were modeled as inflexible joints. Since the real structure is fixed on a bolted down 30-mm-thick steel plate, no displacements and no rotations are assumed at the root. The section definitions, such as tube diameter and wall thickness, are assigned according to measurements taken from the actual structure, which are given in Figure 3. Linear elastic parameters matching those of structural steel were applied in the material model. Further, we considered several mass contributions of the structure in order to achieve a model as close as possible to the actual structure without applying any advanced model updating scheme. These mass contributions are listed in Table 4. The segments were weighed to account for masses not included in the mechanical modes such as paint and weldment material. Subsequently, we calibrated the material density such that the resulting mass of the model matched the weight of the real segments. The mass contributions of the flanges, which connect the segments, as well as a ring located at the top of the uppermost segment (cf. Figure 1) were considered. Further mass contributions arise from the sensors and cables installed on the structure. The mass of the two-sensor setup of each measurement level is represented by point masses at the respective positions in the structure. We accounted for the mass of the cables running from the base of the mast to the respective measurement levels using concentrated masses located at the intersections of the bracings and the leg on which the cables were installed.

The vibration modes and natural frequencies of the structure were computed using the finite element solver *Abaqus*. Figure 5 shows the first four bending and torsional modes. The bending modes all occur in pairs for linearly independent directions of deflection (x and y direction) because of the symmetric geometry of the structure's cross section. However, only the bending modes pointing in x direction are shown in Figure 5.

The lower modes behave as expected for a beam-like structure. However, the higher modes have a more intricate structural dynamic behavior. For example, the upper 10 cm of the legs of each segment lack any bracings, and thus, the parts of the structure near the interconnections of segments have a significantly reduced stiffness. This is especially reflected in the fourth bending mode shape (B4-x), which exhibits a large curvature in the respective locations. Further, B4-x also shows significant excitation of the individual braces.

3 | CHARACTERIZATION OF DYNAMIC PROPERTIES

When establishing a monitoring scheme, one usually needs to characterize the structural dynamic behavior of the system to be observed to select appropriate methods, for example, for system identification. Typically, this characterization is based on assumptions or experience at least to some extent. However, in most cases the monitoring scheme comprises a training phase (see, e.g., Häckell et al.[41]), and therefore, the corresponding observations can be used to validate the assumptions and to develop a comprehensive understanding of the dynamic behavior, which effectively reduces the chances of misinterpretations regarding the structural integrity.

In the context of this article, we want to characterize the dynamic properties of the test structure with the help of the data gathered from August to December, 2020. The goal is to answer the following questions: (i) Is the structure linear or nonlinear? (ii) Are there any exogenous effects that might alter the dynamical behavior? (iii) Is the structure varying over time? (iv) Another open question is whether the damage mechanisms are truly reversible, that is, that the global dynamic properties are recovered once the connection pieces have been removed and set back in place.

TABLE 4 Mass contributions considered in the finite element model

Density (including weldment, paint)	8670 kg/m^3
Flange mass (6 per segment)	0.125 kg
Head mass (ring at top segment)	2.97 kg
Sensor fixture (including accelerometers)	0.387 kg
Cable mass (single accelerometer channel)	0.0356 kg/m

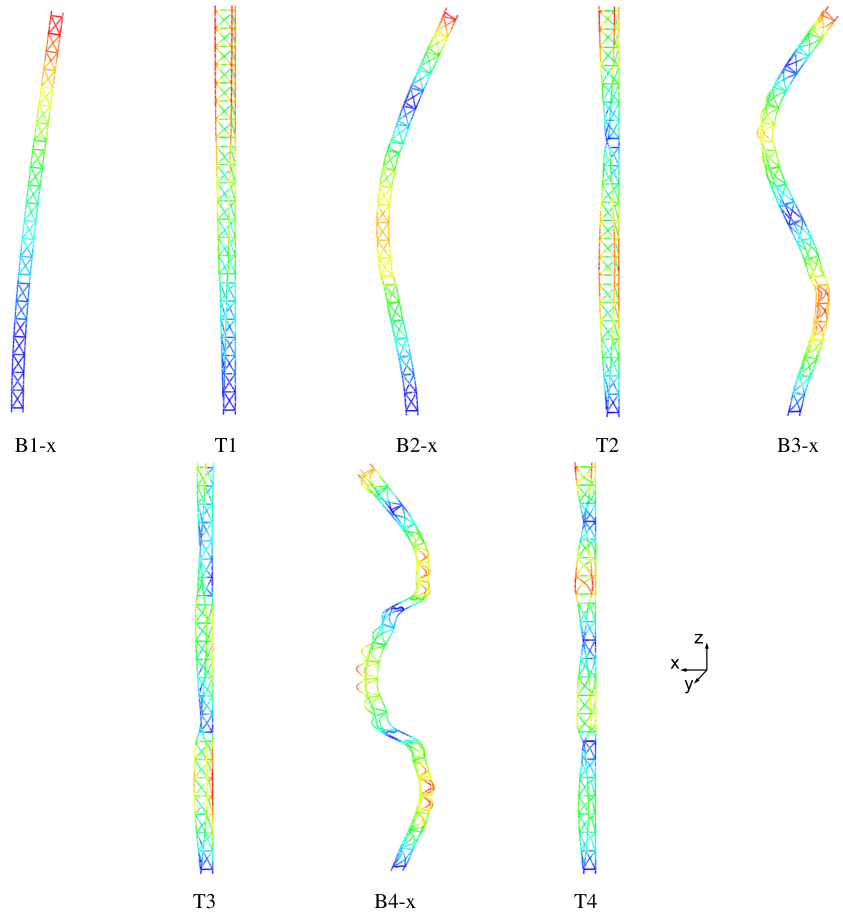

FIGURE 5 Finite element results for bending mode shapes of the healthy state

For modeling dynamic processes stemming from ambiently excited structures under environmental and/or operational variability, it is advisable to distinguish between short-term and long-term scale, as some properties mentioned in the questions before might appear, or become relevant, in either of these temporal cases. We will give some recommendations for modeling toward the end of this section. Note that the mentioned time scales (short-term and long-term) cannot be defined generally. For the test structure, we refer to short-term scale when considering the 10-min data blocks.

3.1 | Modal analysis

For now, we assume that the test structure can be modeled as a linear time-invariant (LTI) system given the 10-min acceleration measurements. For structures like the lattice mast, that is an assumption, which is readily made.[42] It implies that no exogenous effects exist, which alter the lattice mast significantly during this time. Otherwise, estimation errors of the modal parameters would increase.[43] We computed natural frequencies, damping ratios, and mode shapes of the test structure under healthy conditions every 30 min from August 1 until October 12, 2020. Therefore, the Covariance-Driven Stochastic Subspace Identification (SSI-COV)[44,45] was applied. To distinguish between spurious and physical eigensolutions, stabilization diagrams[46] were utilized. In the proceeding sections, the underlying presuppositions of linearity and time invariance shall be investigated.

For the SSI-COV, covariances were computed based on an inverse Fourier transform of the power spectral density (PSD) matrices of the acceleration data. The PSDs were estimated using Welch's method[47] with a window length of 1 min and an overlap of 50%. We chose these values based on experience. A Blackman window was applied to each data block to reduce leakage effects. The number of frequency points was set equal to the number of data points, leading to a frequency resolution of 0.0167 Hz. To regard the character of the measured acceleration data, a plot of the three first

singular values of the PSD matrices versus frequency is given in Figure 6. The frequency axis is cut off at 120 Hz, as this range contains the vibration modes regarded later on.

From there, it can be seen that the first singular value represents the major dynamic response of the structure. In many cases, this component predominantly embodies closely spaced modes, for example, around 16 Hz. However, the second and third singular value play a significant role in this regard as well.

Concerning the modal analysis, all identified natural frequencies for the range of 0 to 120 Hz are given in Figure 7. By *natural frequency*, we refer to the damped eigenfrequencies[48] throughout this article, when not stated otherwise.

To differentiate separate vibration modes, we developed and applied a simple clustering algorithm to all identified natural frequencies from 0 to 200Hz and their corresponding mode shapes using the settings in Table 5. The values therein were chosen in such a way that, on the one hand, significant deviations of natural frequencies due to EOVs were allowed and, on the other hand, modal affinity assured (see value for Modal Assurance Criterion[49] [MAC] and frequency difference of clusters).

That leads to the identification and separation of the first 15 modes listed in Table 6.

Note that the identification of more than these vibration modes is feasible without great effort. However, because of the limited spatial resolution by the given sensor layout, a characterization, as pursued in Table 6, is hard to achieve for higher modes. Even for some of the considered modes, for example, for the first five torsional modes, a clear

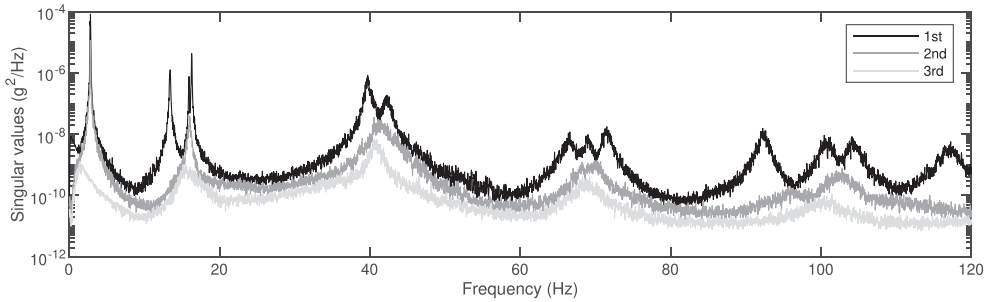

FIGURE 6 First three singular values of power spectral density (PSD) matrices ($\Delta f = 0.0333$ Hz) of acceleration measurements

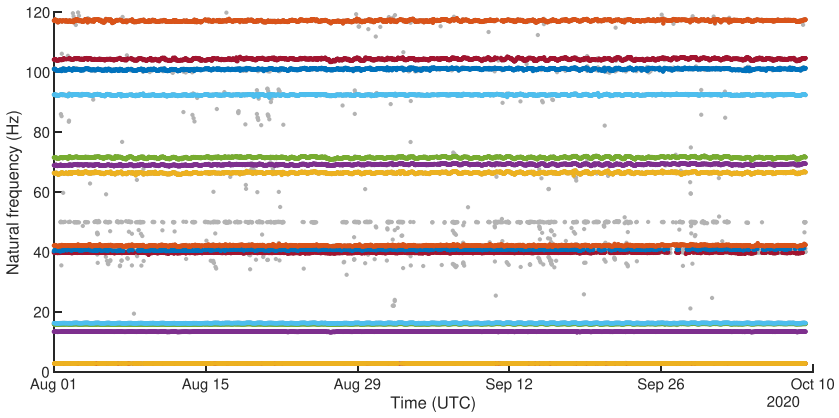

FIGURE 7 All identified and classified natural frequencies of the lattice tower from 0 to 120 Hz (unclassified frequencies in gray)

TABLE 5 Criteria for modal clustering of identified modes based on 10-min data sets

Criterion for modal clustering	Value
Min. MAC value within cluster	0.95
Max. absolute frequency deviation within cluster	1 Hz
Min. absolute frequency difference between cluster's mean frequencies	0.02 Hz

classification is only possible with help the of the finite element results summarized in Section 2.6. Finally, in Figure 8, the first five bending mode shapes in *y* direction are given for illustration purposes.

To make the results comparable to the numerical solutions, linear interpolation was used to generate deformed plots of the structure. Since there are only nine measurement levels in the structure, the mode shapes for B4-y and B5-y are not fully resolved.

In Table 6, values for the natural frequencies of the simulated model are given as well. Compared to the identification results, they feature only minor deviations. We also computed the MAC values given the mode shapes from system identification and numerical simulation, which are also given in Table 6. In some cases, the direction of vibration of the

TABLE 6 Description of first 15 vibration modes and frequencies obtained using SSI-COV and modal clustering using parameters given in Table 5, and comparison to numerical results

Index	Average natural frequency, Aug. 1 to Oct. 12, 2020	Natural frequency from simulation	MAC, simulation versus identification (after rotation)	Type of vibration mode (dominating direction)	Identifier
1	2.76 Hz	2.95 Hz	0.976 (0.999)	1st bending mode (*y*)	B1-y
2	2.81 Hz	2.95 Hz	0.977 (0.998)	1st bending mode (*x*)	B1-x
3	13.40 Hz	14.11 Hz	0.995 (0.995)	1st torsional mode	T1
4	15.94 Hz	17.16 Hz	0.988 (0.994)	2nd bending mode (*y*)	B2-y
5	16.28 Hz	17.15 Hz	0.983 (0.984)	2nd bending mode (*x*)	B2-x
6	39.78 Hz	41.74 Hz	0.964 (0.968)	2nd torsional mode	T2
7	40.76 Hz	44.32 Hz	0.651 (0.794)	3rd bending mode (*y*)	B3-y
8	42.14 Hz	44.18 Hz	0.973 (0.985)	3rd bending mode (*x*)	B3-x
9	66.40 Hz	68.47 Hz	0.623 (0.627)	3rd torsional mode	T3
10	69.15 Hz	71.84 Hz	0.558 (0.558)	4th bending mode (*y*)	B4-y
11	71.51 Hz	70.95 Hz	0.910 (0.922)	4th bending mode (*x*)	B4-x
12	92.40 Hz	94.38 Hz	0.942 (0.944)	4th torsional mode	T4
13	100.98 Hz	103.51 Hz	0.809 (0.939)	5th bending mode (*y*)	B5-y
14	104.33 Hz	104.29 Hz	0.790 (0.963)	5th bending mode (*x*)	B5-x
15	117.16 Hz	120.44 Hz	0.907 (0.935)	5th torsional mode	T5

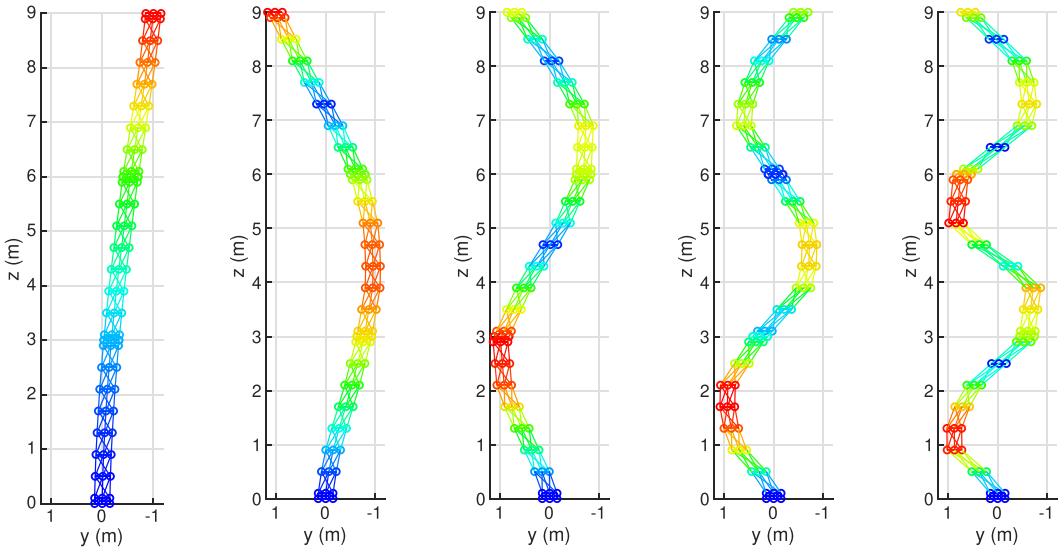

FIGURE 8 Bending mode shapes in *y* direction (B1-y [left] to B5-y [right]), as identified from the measurement data using Covariance-Driven Stochastic Subspace Identification (SSI-COV)

compared mode shape pairs was obviously deviating. This is why we computed a second value for the MAC after rotating the mode shapes in a least-squares sense. The latter values show a good resemblance of the simulation model and the actual structure. However, several modes of the finite element model exhibit a strong coupling between bending and torsion, which lead to low MAC values when compared to the identified mode shapes (cf. B3-y, T3, and B4-y). We want to emphasize again that a calibration of the finite element model might be useful, however, as we provide the nominal model in addition to the measurement data, the corresponding numerical results are presented here.

An analysis of the evolution of the natural frequencies reveals that the global dynamics of the test structure undergoes significant changes when observed over time. To this end, we exemplarily show the progress of modes B2-y and B2-x in Figure 9.

The main driver of this behavior seems to be the material temperature, as day-night cycles are apparent. We will examine this property in depth later on.

3.2 | Linearity and nonlinearity

We generally assume the lattice mast to be a linear dynamic system, since the test structure is a steel construction and the aerodynamic forces are small compared to the bearing capacity. However, two properties could introduce a significant dependence with respect to the magnitude of excitation. First, amplitude-dependent dynamics of buildings under wind loading have been reported extensively in the literature, see, for example, previous works,[50–52] and the references therein. Generally, this is exhibited by an increase in damping and a decrease in natural frequencies. A reason for that might be the aerodynamic damping that increases with stronger winds, and which could cause a decrease of natural frequencies. On contrary, Tamura[53] explains the joint variation of damping and natural frequencies, which results in a softening, with the help of the so-called *stick-slip model*. It is worth mentioning that a softening has even been reported for prestressed structures, where the opposite (hardening) would have been expected.[54] Second, as the tower is erected on a block foundation, amplitude-dependent material properties of the soil could affect the global dynamics as well.[53,55]

To investigate a possible nonlinearity in terms of amplitude dependence, we consider the same measurements and identified natural frequencies as before. From the previous section, we know that temperature variations due to day-night cycles have an obvious effect on the dynamics of the test structure, which is a typical phenomenon.[56–58] To limit this possible source of variation, identification results were considered that refer to data sets associated with a mean material temperature of 14.2 to 16.2°C. We chose this temperature range, as most data sets were acquired during these conditions. Further, we assumed that a material temperature deviation of 2 K has an insignificant effect on the modal properties. In Figure 10, the identified natural frequencies of mode B2-x are plotted over time. Additionally, the maximum wind speed for the corresponding 10-min data sets is displayed underneath.

Even though the temperature deviations only amount to 2 K, significant variations of the natural frequencies can be observed in this figure. Here, two periods are of special interest: a few days before August 29, and the week before October 10. During this time, the maximum wind speed frequently exceeded 10 m s^{-1}. Accordingly, the identified natural frequencies dropped significantly. Besides the displayed natural frequencies in Figure 10, this phenomenon can also be observed for other modes.

To rule out other sources for these variations, several dependency plots are given for the identified natural frequencies and the acquired meteorological data (see Table 2) averaged over the 10-min interval of the corresponding acceleration data. Unlike the other meteorological data, the maximum value instead of the average value was considered for maximum wind speed. In addition to the meteorological data, the mean material temperature was considered, which was measured directly at the lattice mast. In Figure 11, an exemplary dependency plot is given for the mode B2-x.

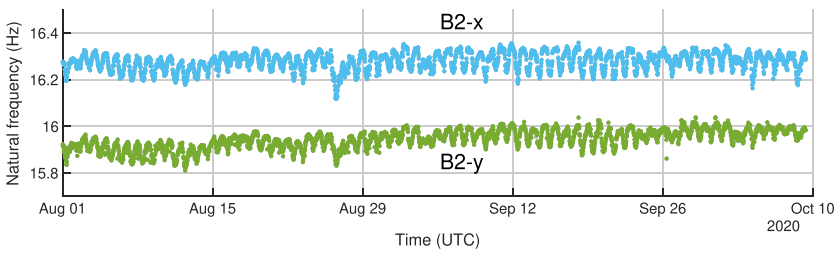

FIGURE 9 Evolution of natural frequencies of vibration modes B2-y and B2-x

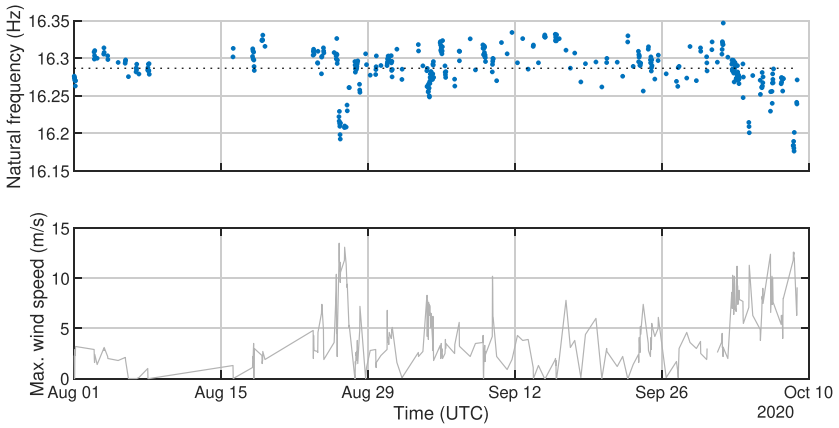

FIGURE 10 Natural frequencies for mode B2-x, and maximum wind speed over time (material temperature (MT) from 14.2°C to 16.2°C); mean natural frequency mode cluster in dotted line

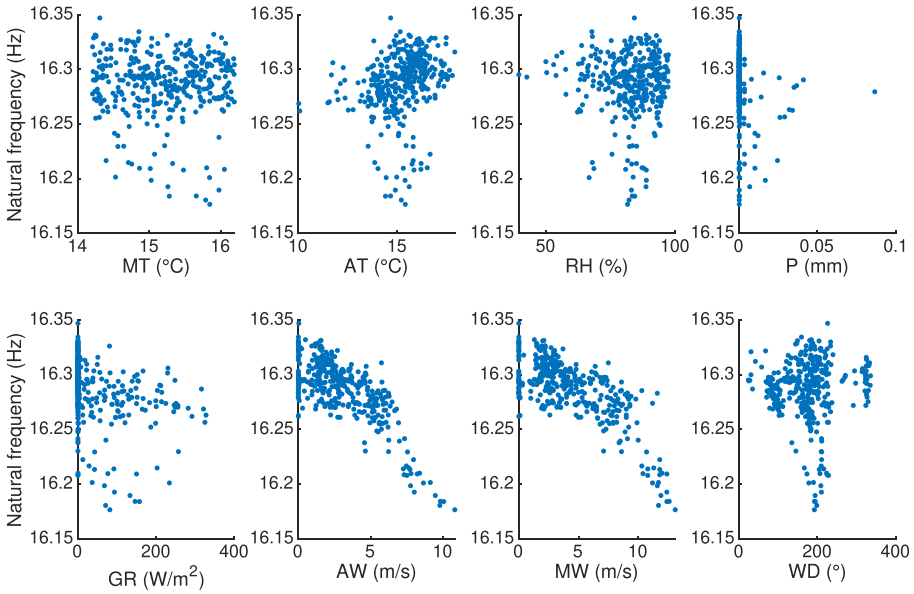

FIGURE 11 Dependency plots of natural frequencies of mode B2-x versus meteorological data and material temperature (MT); data are filtered according to MT (14.2–16.2°C). For abbreviations, see Table 2

Therein, a decreasing trend of the identified natural frequency is visible with respect to rising wind speeds. Further, it can be seen that the selected window of material temperature has no significant varying effect on the regarded natural frequency. Amplitude-dependent natural frequencies usually come along with amplitude-dependent damping.[50,53] This can be observed here as well by regarding Figure 12.

Besides the subplots for natural frequency or damping ratio, respectively, versus average (AW) and maximum wind (MW) speed, other combinations appear to feature dependent relations as well. In the cases of natural frequency/damping ratio versus sum of precipitation (P) or global radiation (GR), this can be traced back to fewer identification results for phases with high global radiation or much precipitation. Similarly, this pertains to the relationship of natural frequency/damping ratio and wind direction (WD), where most realizations exist when the wind was coming from 200° (south-south-west).

We want to close this section with a final remark. When considering the undamped natural frequencies[48] for the investigations of this section, the amplitude dependence still pertains. This leads to the conclusion that the natural frequencies are indeed amplitude-dependent. However, the reason could also be a poor estimation of damping, which is considered as challenging within the OMA community.[59] It would be interesting to perform the estimation of damping using different modal identification techniques. However, this is beyond the scope of this paper.

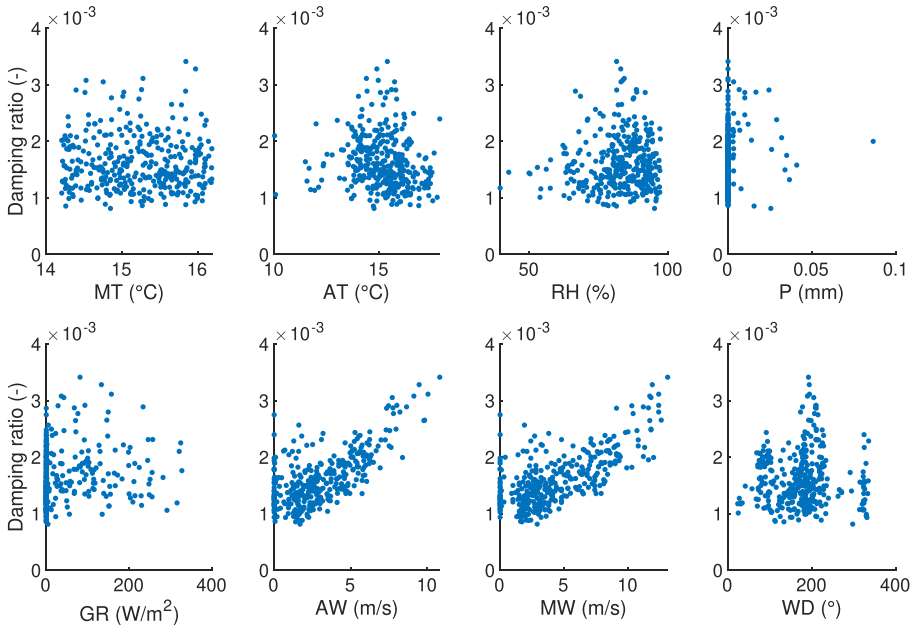

FIGURE 12 Dependency plots of damping ratios of mode B2-x versus meteorological data and material temperature (MT); data are filtered according to MT (14.2–16.2°C). For abbreviations see Table 2

3.3 | Dependence on environmental conditions and time

In the previous sections, we reported that the test structure features amplitude-dependent dynamics, which can be observed in a decrease of natural frequencies and an increase of damping ratios with rising wind speeds. For the relevant investigations, we modeled the test structure as an LTI system using the SSI-COV technique. At the same time, we presumed that the dynamics of this system are temperature-dependent, and therefore, we only considered data sets for similar material temperatures. If either temperature or wind speed variations were high during the considered 10-min measurements, the assumption of stationary dynamics could be violated.

This shall be further investigated, and therefore, the dynamical behavior is assessed by observing the frequency content of an exemplary 10-min acceleration data set under particularly high variations of temperature or maximum wind speed. First, we consider the same period as earlier (August 1 until October 12, 2020) and find a particularly high standard deviation of material temperature within 10-min data blocks of 1.7°C on August 29 (11:56h–12:06h). During this time, the maximum wind speed varied moderately, namely, between 3.1 and 5.6 m s^{-1}. For a short-time analysis, we extracted nine subsequent blocks, each block belonging to a full minute. We then applied the Bayesian Operational Modal Analysis (BAYOMA) technique[60,61] to each of these chunks to estimate the natural frequencies as well as the uncertainty associated with them. To apply BAYOMA, the FFT was computed with a frequency resolution of 0.0167 Hz. To observe changes in frequency, we considered the bending mode B2-x. The corresponding nine natural frequency values as well as the material temperature are plotted over time in Figure 13.

Therein, slight variations of the natural frequency can be observed with respect to the changing material temperature. It seems that the dependency of natural frequency on temperature explored in the long-term analysis associated by Figure 16 also manifests itself in short observation periods although the effect is not particularly distinct.

We conducted a similar analysis regarding the variation of wind speed. Therefore, we considered the acceleration of the data set acquired on October 6, 2020 (07:41h–07:51h). During this time, the maximum wind speed varied between 6 and 12.4 m s^{-1} and the standard deviation of the material temperature amounted to approximately 0.07°C ranging from 11.93°C to 12.12°C. The results of the short-term frequency tracking of mode B2-x can be found in Figure 14.

Significant variations of the resonance frequency with respect to the measured maximum wind speed are observable during the regarded 10-min interval.

Especially Figure 14 but also Figure 13 show that a dependency on environmental conditions is apparent during measurement intervals of 10 min when strong variations of these effects occur. However, to further assess these findings, they should be compared to a short-time modal analysis using data that was acquired under moderate variations

of wind speed and temperature. Such a case can be found on October 4th, 2020 (03:42h–03:52h). At that time, the material temperature ranged from 2.8°C to 3.7°C resulting in a standard deviation of approximately 0.02°C. The variation of the maximum wind speed was small as well, as can be seen in Figure 15.

In the latter figure, no significant variations of the depicted natural frequency can be observed. Comparing these results to the ones contained in Figures 13 and 14 emphasizes the altering effect of temperature and especially wind speeds on the dynamic behavior of the girder mast on a short-term scale. It follows that a general modeling of the girder mast as LTI system must be associated with certain modeling errors when 10-min data sets are employed that were acquired under strongly varying wind speeds but also temperature. Nevertheless, since these instances happen rarely, such a procedure seems legitimate anyway. We will take up on this topic in Section 3.4.

We now want to investigate the temperature effects on the global dynamics of the test structure over long periods. To this end, we again consider acceleration data acquired under healthy conditions from August 1 until October

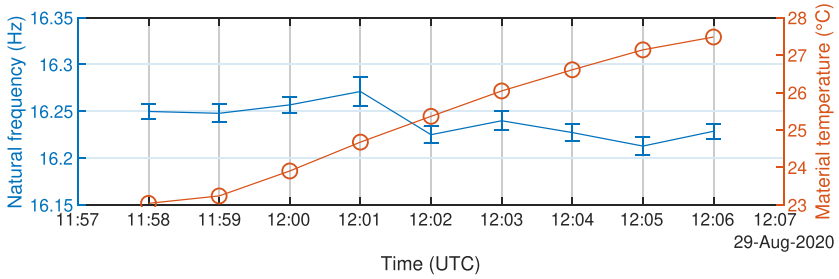

FIGURE 13 Short-term frequency tracking of natural frequency of B2-x by Bayesian Operational Modal Analysis (BAYOMA) for the case of maximum material temperature variation and slightly varying maximum wind speeds (3.1 to 5.6 m s^{-1}). Vertical bars depict standard deviations of the point estimates. Identification for full minutes only

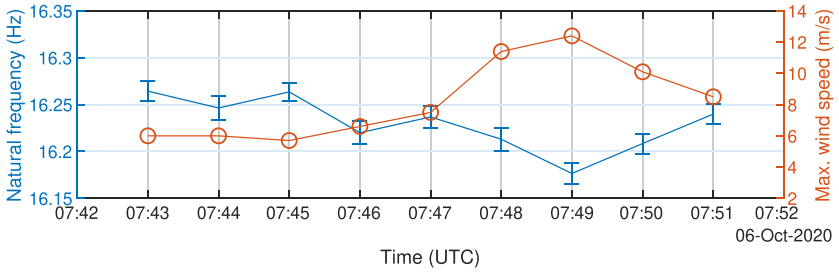

FIGURE 14 Short-term frequency tracking of natural frequency of B2-x by Bayesian Operational Modal Analysis (BAYOMA) for the case of maximum wind speed variation and quasi-constant material temperature 11.93°C to 12.12°C. Vertical bars depict standard deviations of the point estimates. Identification for full minutes only

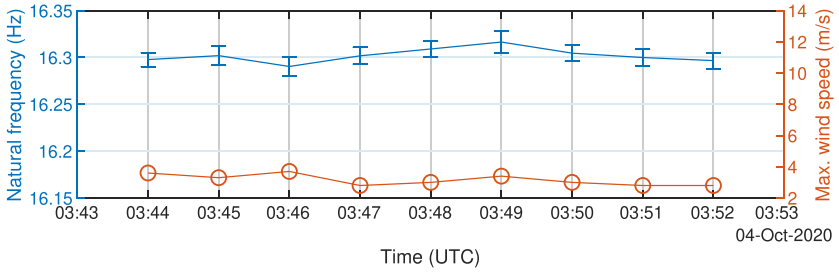

FIGURE 15 Short-term frequency tracking of natural frequency of B2-x by Bayesian Operational Modal Analysis (BAYOMA) for the case of moderate variations of maximum wind speed and material temperature (2.8° to 3.7°C). Vertical bars depict standard deviations of the point estimates. Identification for full minutes only

12, 2020, but this time irrespective of the underlying temperature. Contrary to the investigations behind Figures 11 and 12, we filtered the modal results with respect to the maximum wind speed, which we allow to vary between 2 and 7 m s^{-1}, the material temperature is allowed to vary freely. By that, we want to disregard the amplitude dependence of natural frequencies and damping ratios, as described earlier. However, the range of maximum wind speed was chosen relatively large to take into account a great amount of identification results. The effect of temperature variation can be observed in Figure 16.

Therein, the natural frequency of mode B2-x is plotted versus the meteorological data and material temperature. Clearly, a strong temperature dependence exists, which appears linear for the regarded temperature range. Such a linear relationship pertains to all identified modes. Figure 16 also displays a dependence of natural frequency and relative humidity. However, this is deceptive, as the relative humidity and air temperature are correlated. Further, a slight decreasing trend of the damped natural frequency with rising wind speeds is still visible, although it is masked behind temperature variations. Apparently, the range of maximum wind speed from 2 to 7 m s^{-1} was chosen slightly too large. However, as the effect of varying temperature on the natural frequencies is predominant, this selection is justified.

Additionally, the corresponding identified damping ratios are presented in Figure 17.

As expected, no significant temperature dependence can be recognized here. As before, slight trends of the damping ratio with respect to the wind speed can be recognized. That roots back to the amplitude-dependent dynamics of the test structure, which is not entirely disregarded by the large range of the wind speeds considered.

During our investigations, we realized that not only the natural frequencies do change with varying temperature but so do the mode shapes. This phenomenon is typical for structures with closely spaced modes that result from symmetric geometry and which are *found to be sensitive to physical conditions*.[62] This behavior can be observed exemplarily for mode B2-x in the upper plot of Figure 18, where MAC values are depicted over the measured material temperature. For this computation, we chose the reference eigenvector as the one closest to the nominal mean material temperature at approximately 20°C.

As reported in the literature,[63] eigenvectors of closely spaced modes like B2-y and B2-x tend to rotate within the subspace spanned by these vectors. Therefore, the whole subspace should be considered instead of the individual mode shapes, and consequently, the classical MAC is not entirely suitable. Extensions based on the subspace of eigenvector pairs can be used instead,[64] which should be considered in future investigations.

To disregard the effect of rotation, we computed alternative values for the MAC of mode B2-x based on the modal amplitudes for the sensors pointing in the dominating x direction, which are given in the lower plot of Figure 18. Therein, a clear trend with respect to varying material temperature is still apparent. To investigate this effect, we present the normalized modal amplitudes associated with the sensors oriented in x direction plotted over the material

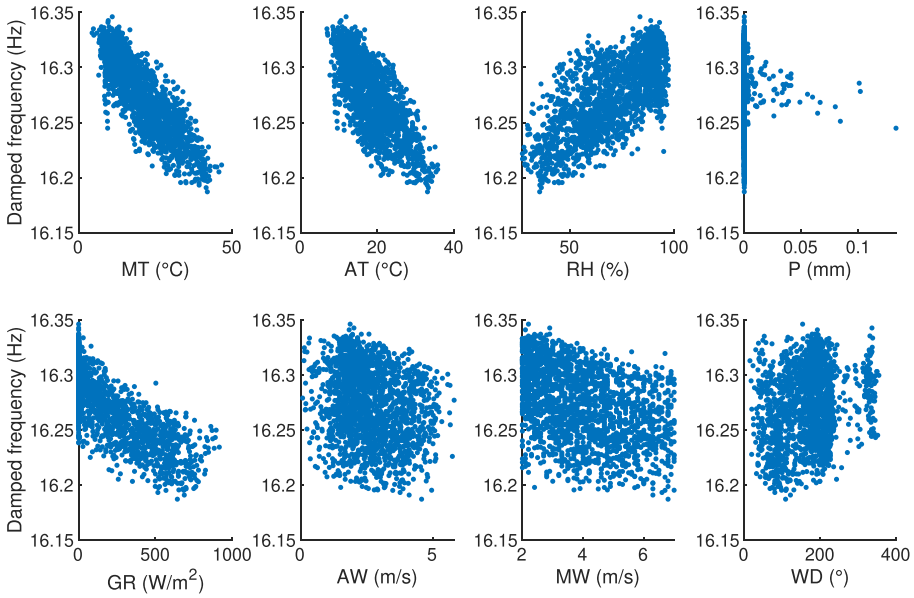

FIGURE 16 Dependency plot of natural frequency for mode B2-x versus meteorological data and material temperature (MT); data are filtered according to MW (2–7 m s^{-1}). For abbreviations see Table 2

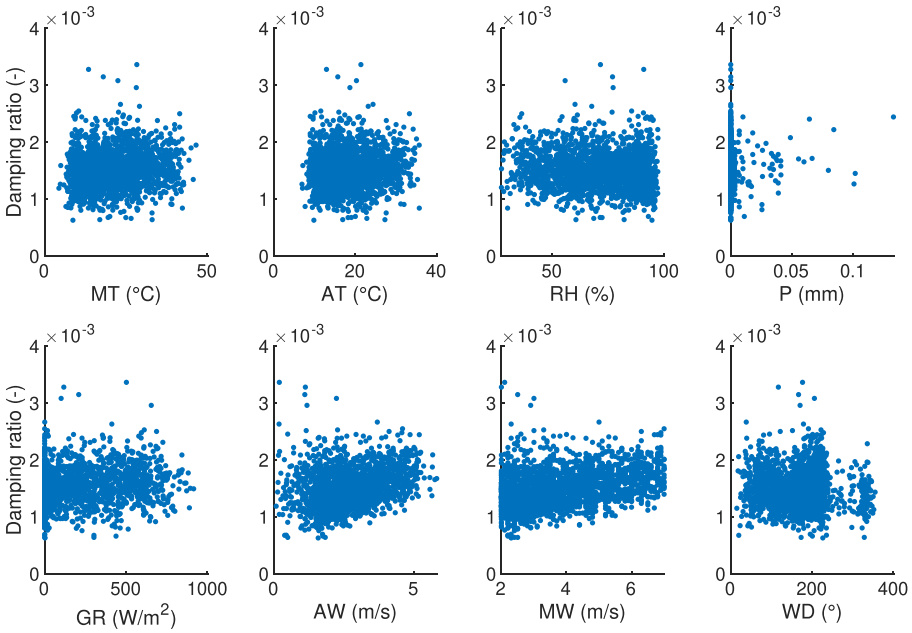

FIGURE 17 Dependency plot of damping ratio for mode B2-x versus meteorological data and material temperature (MT); data are filtered according to MW (2–7 m s^{-1}). For abbreviations see Table 2

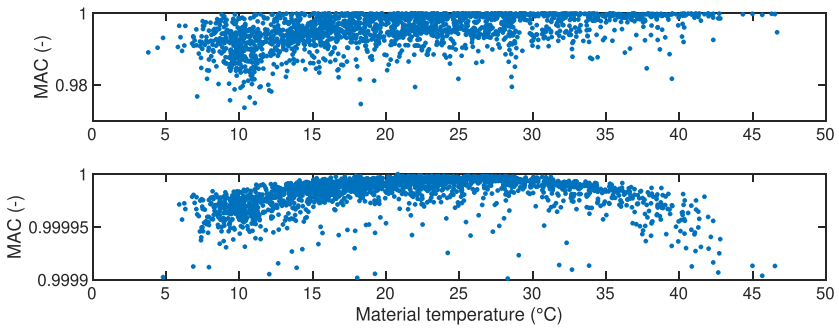

FIGURE 18 Modal Assurance Criterion (MAC) values versus temperature for eigenvectors of B2-x (top), and MAC values versus temperature for eigenvectors of B2-x considering only sensors in *x* direction (bottom); reference eigenvector for material temperature of approximately 20°C

temperature in Figure 19. For that, the reduced eigenvectors were normalized with respect to their length, and then, all other mode shapes were scaled with the help of the so-called Modal Scaling Factor.[65]

Especially for the larger amplitudes, slight variations with changing temperatures can be observed. That behavior could be caused by an inhomogenous temperature distribution along the height and cross section of the lattice tower.

At last, we want to address the issue of time dependence. The dynamics of many engineering structures, so of the presented lattice tower, is rather dependent on exogenous effects than on time. However, both properties are often hard to distinguish for the following reasons. First, the evolution of exogenous effects is a function of time, and second, the driving exogenous variations might not or cannot be observed. Consequently, it is sometimes irrelevant if a system is interpreted as time-dependent, or as parameter-variant (dependent on exogenous variations). Moreover, from a practical standpoint, the latter matter is often disregarded and the observed system is simply defined as time-invariant if the dynamic properties seem to be constant, or time-variant in the opposite situation. In case of the test structure, we have the chance to observe a variety of environmental influences. That leads to a better understanding of its structural dynamics and enables researchers to model the dynamics as parameter-variant (see, e.g., Avendaño-Valencia et al.[66]). Despite the thorough monitoring of exogenous effects, there exist some sources of variability that could only be classified as time-dependent, or need to be taken into account as uncertainty. (i) First to be mentioned are the damage

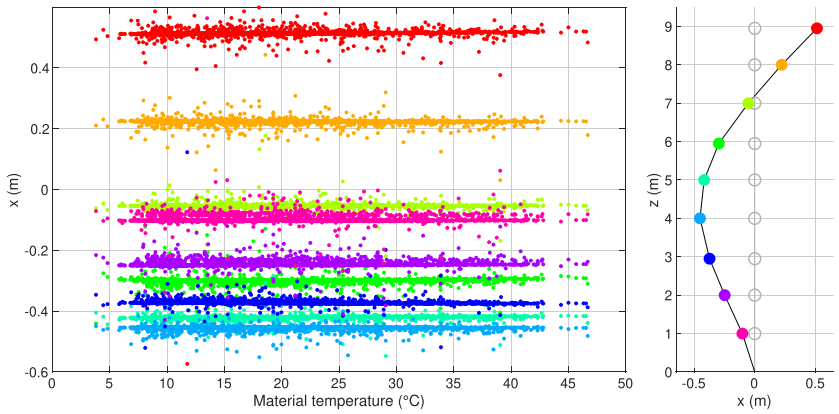

FIGURE 19 Normalized modal amplitudes versus temperature for eigenvectors of B2-x considering only sensors in x direction (left), and reference eigenvector for material temperature of approximately 20°C (right)

mechanisms. Even though the corresponding screw sockets (cf. Section 2.2) were properly tightened and secured when the structure was erected or reset in healthy state, local stiffnesses might change due to settlements or repositionings caused by temperature variations or sudden wind strokes. (ii) During visual examinations, we could observe that the lattice mast has been sought by birds as a place to rest. This increase of mass leads to temporarily lower natural frequencies. (iii) Even though we took special care of the rust protection of the steel construction, corrosion might alter the lattice mast with time, which could result in different dynamic behavior.

3.4 | Modeling dynamics

At this point, we want to summarize the findings from the previous sections and derive some recommendations for the modeling of the structural dynamics on a short- and long-term scale.

The dynamics of the test structure can be described as follows: (i) The structure features nonlinearities in terms of amplitude-dependent natural frequencies and damping. (ii) The natural frequencies and mode shapes vary with the temperature. (iii) In the measurement data considered for this article, no exclusive time-dependent behavior of the structure has been observed.

The previous investigations show that these properties significantly manifest themselves on a long-term scale but also during shorter observation periods (<10 min) when particularly high variations wind speed but also temperature are present. This must be kept in mind when a high modeling precision is pursued. Nevertheless, as the exogenous conditions are typically rather stationary over intervals of 10 min, modeling the test structure as an LTI system based on such observation periods is legitimate. However, on a long-term basis, the test structure must be considered as nonlinear and parameter-variant. Depending on the objective(s) of the long-term analysis, different kinds of methods are applicable. For instance, if one were interested in monitoring the natural frequencies of the test structure, even a linear surrogate model[24] could be identified representing the linear dependence of natural frequency and wind speed or temperature.

4 | RECONSTRUCTING MISSING WIND MEASUREMENTS

We realized that from time to time single wind measurements went missing, which manifests itself in NaN values for the corresponding channels of the meteorological data (AW, MW, WD, see Table 2). While few instances are not problematic, longer periods with absent information are troublesome from an SHM point of view. Especially the maximum wind speed constitutes an valuable parameter that should be considered when the structure is monitored, cf. Figure 11. Because of a sensor defect of the cup anemometer, no wind measurements are available from May 7, 2021 (07:30h) until June 21, 2021 (07:00h). Nevertheless, this data might be recovered with the help of the structural measurements by exploiting correlations observed in times with complete data.

Missing data are a common problem in SHM and is usually approached by determining a surrogate model to estimate the lost samples (cf. Martín-Sanz et al.[58]). Therefore, correlation analyses revealed that the variance of acceleration signals referring to ML 9 (see Figure 3) are most correlated with the maximum wind speed (both considered for 10 min). Notably, and probably because of a better signal-to-noise ratio, the acceleration signals are more suitable for the reconstruction of the maximum wind speed than the strains at ML 10. To suppress the effect of varying wind directions, the absolute value of the 10-min variance of channels *accel09x* and *accel09y* is considered so that

$$\mathrm{var}\{\mathrm{accel09}\} = \sqrt{\mathrm{var}\{\mathrm{accel09x}\}^2 + \mathrm{var}\{\mathrm{accel09y}\}^2},$$

where var$\{\cdot\}$ denotes the variance. The correlation to the maximum wind speed can be observed in Figure 20, where log var{accel09} is plotted versus maximum wind speed. For that, we utilized all data from August 1, 2020 until April 30, 2021 that refer to the structure under healthy conditions. Clearly, applying the logarithm reveals a linear correlation, which is emphasized by the Pearson correlation coefficient of $\rho_P = 0.94$.[67]

Consequently, estimating the maximum wind speed based on 10 min of acceleration data by employing a linear surrogate model seems legitimate. It is worth mentioning that values below 0.5 m s^{-1} most probably do not reflect the actual maximum wind speeds. This suspicion is triggered by the frequency of measurements at 0 m s^{-1}, where at the same time the corresponding accelerations imply higher excitation intensity. This phenomenon could be explained by the resistance or inertia of the cup anemometer to start spinning at lower wind speeds. As mentioned before, the cup anemometer was replaced by an ultrasonic anemometer on June 21, 2021 (07:00h). Measurements with the new anemometer until July 30, 2021 support this conjecture. Instead of reconstructing the wind measurements in the first place, considering log var{accel09}, for example, for data normalization schemes is a valuable option that circumvents the problem of surrogate modeling. However, for the sake of completeness, a possible solution for that is presented in the following.

We derived an estimator for the maximum wind speeds with the help of the Principal Component Analysis (PCA).[68] To this end, we gathered the data comprised of log var{accel09} and maximum wind speed acquired over the typical interval of 10 min on the columns of an $(N \times 2)$-matrix X, with N being the number of data sets. To center this data around zero, we subtracted the mean $\overline{X}$.

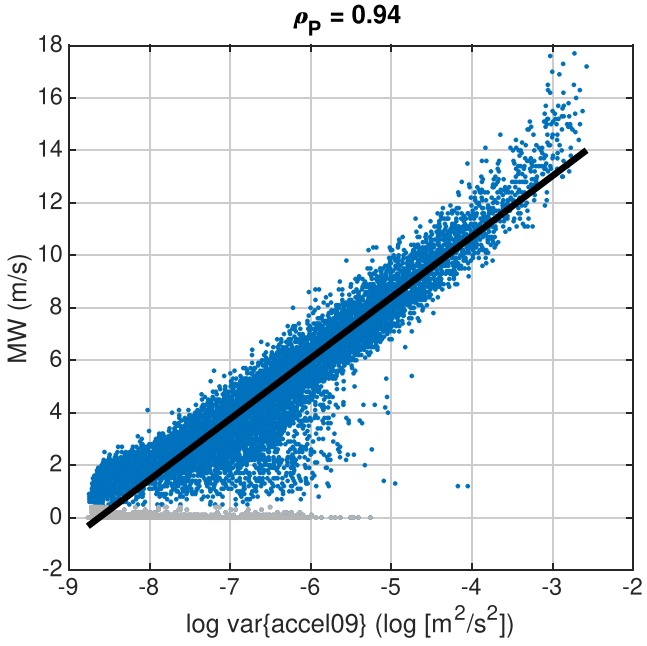

FIGURE 20 Logarithmized variance of measured acceleration (log var{accel09}) at measurement level (ML) 9 versus maximum wind speed for 10-min measurement interval. Principal component (PC) represented by black line, values neglected for Principal Component Analysis (PCA) in gray

To reduce the effects of measurement errors, we neglected measurements referring to a maximum wind speed lower than 0.5 m s^{-1}, which is highlighted in Figure 20 using gray dots. The principal components (PCs) were determined by means of a singular value decomposition (SVD).

A linear function was realized based on the first PC, which refers to the direction of maximum variance. It can be written as

$$\mathrm{MW}_{\mathrm{est}} = m\left(\log\mathrm{var}\{\mathrm{accel09}\} - \overline{X}(1)\right) + \overline{X}(2).$$

Here, $\mathrm{MW}_{\mathrm{est}}$ represents the estimated maximum wind speed and $m, \overline{X}(1)$ (mean $\log\mathrm{var}\{\mathrm{accel09}\}$), and $\overline{X}(2)$ (mean maximum wind speed) are the parameters of the surrogate model that read

$$m = 2.3173,\ \overline{X}(1) = -6.6642,\ \overline{X}(2) = 4.5421.$$

It can be seen in Figure 20 that the PCA is an effective measure of fitting a linear model to the correlated data. The linear function displayed in black clearly follows the direction of maximum variance. Nevertheless, it must be mentioned that estimating the maximum wind speed based on the acceleration signals might result in negative values in the case of low excitation intensity. This issue could be circumvented by rotating or shifting the PC but would lead to a suboptimal linear estimator. Therefore and because of the high variance of $\log\mathrm{var}\{\mathrm{accel09}\}$ below 2 m s^{-1}, we suggest to focus on the data associated with $\mathrm{MW}_{\mathrm{est}} > 2\,\mathrm{m\,s^{-1}}$ when the proposed linear estimation scheme is followed.

Clearly, reconstructing the wind measurements with the help of data acquired at the structure can be problematic if the structural state changes to one that was not considered for the design of the estimator. In other words, the surrogate model should be applicable even when the structure gets damaged. To validate that, we regarded the meteorological data acquired in November 2020, cf. Table 3. This month is particularly suitable for this endeavor as it reflects the girder mast under healthy as well as damaged conditions. The original measurements for a period of 10 min are plotted together with their estimates based on acceleration data in Figure 21. As mentioned before, only maximum wind speeds beyond 2 m s^{-1} were considered.

It can be seen that the linear surrogate model presented before leads to reasonable estimates of the maximum wind speeds for the periods associated with different structural states. In fact, the mean squared estimation errors for the damaged phase are slightly lower than for times when the structure was intact. By that, we conclude that, $\log\mathrm{var}\{\mathrm{accel09}\}$ is suitable to infer the excitation intensity for the girder mast under healthy and damaged conditions as well as reconstructing missing maximum wind speed measurements.

5 | DAMAGE MECHANISMS AND REVERSIBILITY OF GLOBAL DYNAMICS

The reversible damage mechanisms, which are installed at six levels of the lattice mast, are valuable features of the test structure. Therefore, localized damage can be introduced and reversed subsequently, allowing to conduct measurement

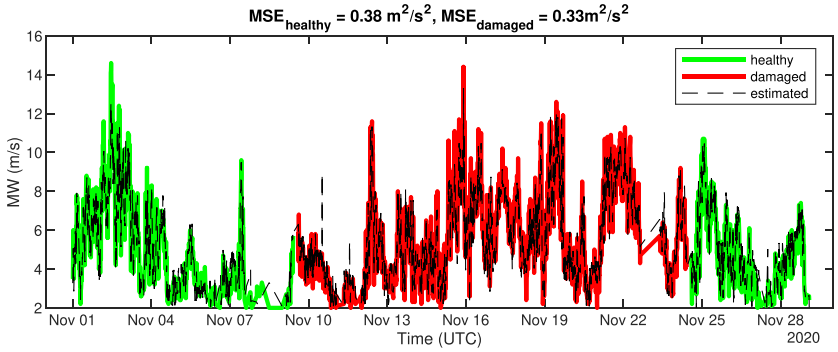

FIGURE 21 Measured and estimated maximum wind speeds for November 2020. Mean squared error (MSE) for data representing the girder mast under healthy and damaged conditions

campaigns under equal reference conditions. From a practical perspective for monitoring or damage detection, it would be desirable if the dynamics of the test structure could be recovered after the system was artificially damaged and repaired. Therefore, long-term measurements of the healthy structure under different environmental conditions could be considered independent of their time of acquisition and their damage and repair history.

During the period from August 1 until July 31, 2021, we damaged the lattice mast six times, as we removed the damage mechanisms completely and continued the continuous data acquisition. Each time, we replaced the missing pieces to bring the test structure back to a healthy state. The corresponding periods and the associated structural states are listed in Table 3.

To investigate the reversibility of the dynamical properties, we considered the data from September 1, 2020 to July 31, 2021, and extracted modal features from acceleration data every 30 min. Again, we applied the SSI-COV method and filtered all the results with respect to a maximum wind speed from 3 to 7 m s^{-1} to disregard the amplitude-dependent effects. The selection of this range is motivated by the findings in Section 3.2, even though changing natural frequencies and damping ratios due to varying magnitudes of wind speed cannot be entirely excluded. Since the considered period overlaps with the phases of missing wind measurements, we estimated the maximum wind speeds for each 10-min data set using the approach proposed in Chapter 4. Figures 22 and 23 show the clustered natural frequencies for mode B2-x over time and air temperature, as well as MAC values versus air temperature. For the latter, the reference eigenvector is given by the first identification result. Values referring to healthy conditions before and after damaging are grouped in separate clusters and depicted in different colors. The cluster associated with the original state (until October 13, 2020) is presented in either plot in cyan color for comparison. Results referring to the damaged structure are plotted in gray. For clustering, we used the same settings as before in Section 3.1 given in Table 5.

In Figure 22, three things can be observed:

- The first repair led to a stiffening of the structure manifested in higher natural frequencies for similar temperatures. The proceeding repairs led to more similar states.
- Damage at different positions has significantly different effects on mode B2-x. From October 13, 2020 until October 27, 2020, all damage mechanisms were removed at DAM 6, see Figure 2, which led to a strong decrease of the regarded natural frequency. When introducing damage at higher positions, this effect diminishes.
- The values of the natural frequency vary strongly within the red cluster (November 24, 2020 until March 18, 2021). This can be explained by the formation of ice at the girder mast. Depending on the amount and location, this might result in stiffening or softening of the structure.

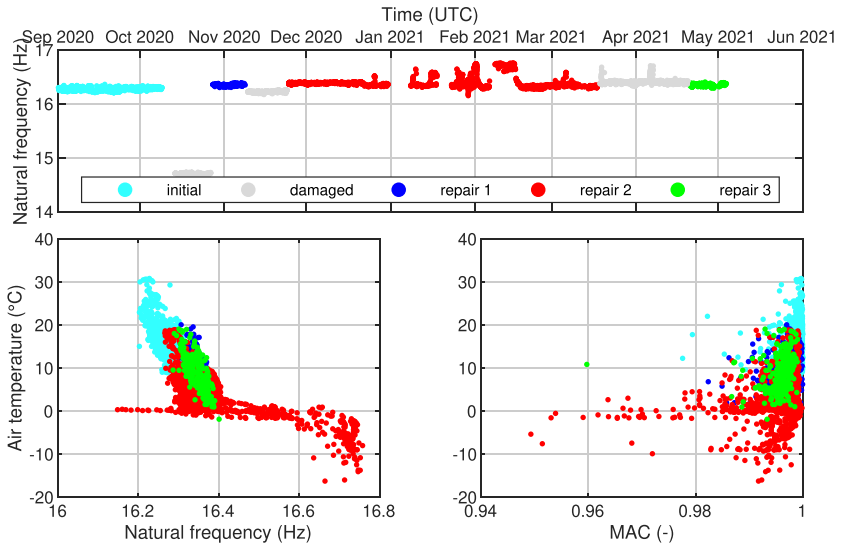

FIGURE 22 Identified natural frequencies of mode B2-x under healthy conditions clustered before and after repair from September 1, 2020 until May 4, 2021. Natural frequencies over time (top), and natural frequencies (bottom left) and Modal Assurance Criterion (MAC) values (bottom right) versus air temperature. Data are filtered according to MW_{est} (3 - 7 ms^{-1}); initial state in cyan

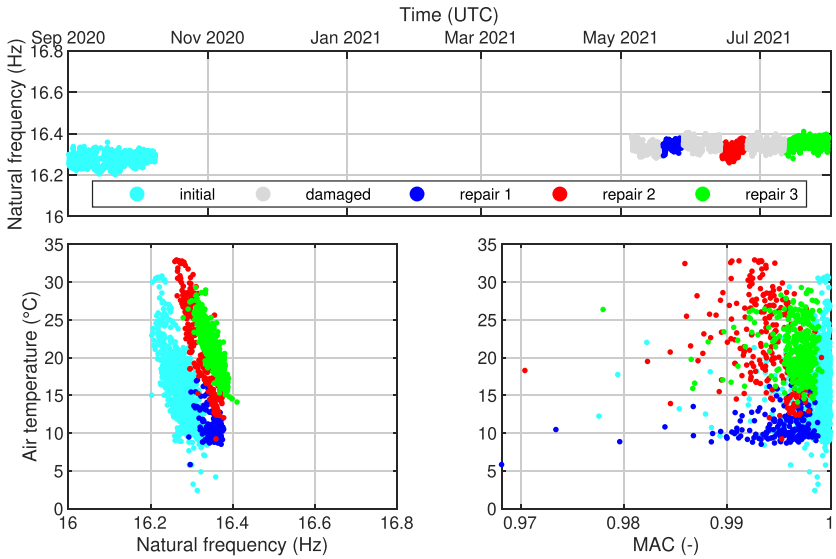

FIGURE 23 Identified natural frequencies of mode B2-x under healthy conditions clustered before and after repair from May 19, 2020 until July 31, 2021. Natural frequencies over time (top), and natural frequencies (bottom left) and Modal Assurance Criterion (MAC) values (bottom right) versus air temperature. Data are filtered according to MW_{est} (3–7 m s^{-1}); initial state in cyan

As mentioned before, Figure 23 is dedicated to the period after May 4, 2021, which covers the minor damage cases, and the corresponding repairs, see Table 3. Nevertheless, the cluster depicted in cyan color, referring to the original state, is presented therein as well. In Figure 23, the following things can be observed:

- Repairing the structure leads to slightly different states that is manifested by different natural frequencies and MAC values for similar temperatures. The original state depicted in cyan color differs significantly in terms of these measures.
- The effect of the considered minor damages on the natural frequency of mode B2-x is not visible in this depiction. Identifying these damages is clearly more challenging than the ones associated with Figure 22.

Given these findings, we can conclude that recovering the initial global dynamics of the girder mast is not entirely feasible. Although in most cases, the prior healthy state could be restored to a reasonable extent, the dynamics varied when compared to the initial state. To enable the usage of all healthy data for data normalization, the effect of repair should be taken into account, e.g. by considering strategies as presented in.[69]

6 | CONCLUSION AND OUTLOOK

As for most engineering fields, the practical applicability and effectiveness of methods utilized in the context of vibration-based SHM can only be truly evaluated in scenarios closest to real-life applications. Therein, a wide spectrum of uncertainties and difficulties need to be considered. In the endeavor of finding suitable sources for validation, some experiments at genuine structures have been conducted. Most of them were characterized as benchmark studies because of a liberal data policy. Unfortunately, these tests are particularly rare, often the test campaigns are short so that little environmental variability is captured,[32] and can not be repeated, as the investigations end with the demolition of the structures.[22,32]

Therefore, in the present article, a test structure was presented, documented, and characterized that constitutes a real-life benchmark for vibration-based SHM. It comprises a lattice mast that features a reasonable degree of complexity and is located outdoors. Hence, it is exposed to all kinds of natural environmental variability. The mast is equipped with a data acquisition system and sensors continuously measuring acceleration, strain, and temperature. These measurements go along with the acquisition of meteorological data at a second mast standing nearby. Most importantly, the test structure comprises reversible damage mechanisms at six levels with three removable braces at each level. All data is

provided in an open-access repository and will be extended regularly. The benchmark structure was established to help researchers to develop, test, and validate methods and strategies for vibration-based SHM, and to set a common baseline for performance and robustness assessment. In this contribution, we characterized the structural dynamics of the test structure based on the first five months of data. Thereby, we identified an amplitude-dependent behavior manifesting itself in alternating natural frequencies and damping with respect to varying wind speeds. The first 15 vibration modes were classified and compared to numerical results from a finite elements analysis. Based on modal properties, we investigated the reversibility of the global dynamics after multiple activation and reactivation of the damage mechanisms, where the reversibility was confirmed.

In the future, damage tests with minor severity will be conducted to particularly support the research in the field of damage localization and quantification. To this end, all six damage levels will be considered and the damage mechanisms shall be activated by loosening the screw sockets but keeping the corresponding pieces in place so that the mass properties are conserved. These measurement campaigns will start in Summer 2022. Until then, data of the healthy structure is gathered to create a solid baseline representing a wide range of environmental variability. The open-access repository will be progressively extended with more data.

ACKNOWLEDGEMENTS

If it had not been for the Institute of Meteorology and Climatology of Leibniz University Hannover, the planning, installation, and maintenance of the test structure would not have been possible. Much credit goes to Ulrich Meyer, Prof. Groß, Prof. Seckmeyer, Prof. Raasch, and Dipl.-Geophys. Holger Schilke. We humbly appreciate their support and dedication.

The authors would further like to thank the Leibniz University IT Services (LUIS) for facilitating the upload of the large amount of data associated with LUMO.

This research has been financed by the Federal Ministry of Economic Affairs and Energy of the Federal Republic of Germany (project: German Research Facility for Wind Energy–Phase 2, FKZ 0325936I) and Deutsche Forschungsgemeinschaft (project: SFB 1463–Integrated Design and Operation Methodology for Offshore Mega-structures). We would like to gratefully acknowledge their support. Open Access funding enabled and organized by Projekt DEAL.

AUTHOR CONTRIBUTIONS

Stefan Wernitz: conceptualization, data curation, formal analysis, investigation, methodology, project administration, software, validation, visualization, writing – original draft preparation, writing – review & editing. **Benedikt Hofmeister:** conceptualization, data curation, formal analysis, software, visualization, writing – original draft preparation, writing – review – editing. **Clemens Jonscher:** conceptualization, data curation, formal analysis, software, writing – review & editing. **Tanja Grießmann:** funding acquisition, project administration, resources, supervision, writing – review & editing. **Raimund Rolfes:** funding acquisition, resources, supervision, writing – review & editing.

DATA AVAILABILITY STATEMENT

Data are openly available in a public repository that issues datasets with DOIs.

ORCID

Stefan Wernitz https://orcid.org/0000-0001-9549-5197
Benedikt Hofmeister https://orcid.org/0000-0003-2615-5521
Clemens Jonscher https://orcid.org/0000-0002-8456-9231

REFERENCES

1. Doebling SW, Farrar CR, Prime MB, Shevitz DW. Damage identification and health monitoring of structural and mechanical systems from changes in their vibration characteristics: a literature review. Los Alamos National Laboratories, 1996. https://www.osti.gov/biblio/249299
2. Rytter A. Vibrational based inspection of civil engineering structures. *Ph.D. Thesis*. Denmark; 1993.
3. Farrar CR, Park G, Allen DW, Todd MD. Sensor network paradigms for structural health monitoring. *Struct Control Health Monit*. 2006; 13(1):210-225. doi:10.1002/stc.125
4. Farrar CR, Worden K. *Structural Health Monitoring: A Machine Learning Perspective*: Wiley; 2012.

5. Deraemaeker A, Worden K. *New Trends in Vibration Based Structural Health Monitoring*. Berlin Heidelberg: Springer Science & Business Media; 2012.
6. Fasel TR, Sohn H, Farrar CR. Application of frequency domain ARX models and extreme value statistics to damage detection. In: Liu S-C, ed. *Smart Structures and Materials 2003: Smart Systems and Nondestructive Evaluation for Civil Infrastructures*, Vol. 5057: SPIE; 2003: 145-156. doi:10.1117/12.482715
7. Figueiredo E, Park G, Figueiras J, Farrar C, Worden K. Structural health monitoring algorithm comparisons using standard data sets. Los Alamos National Laboratories; 2009.
8. Vicario F, Phan MQ, Betti R, Longman RW. Okid via output residuals: a converter from stochastic to deterministic system identification. *J Guid, Control, Dyn*. 2017;40(12):3226-3238. doi:10.2514/1.G001786
9. Wernitz S, Pache D, Grieß mann T, Rolfes R. Performance of an h-infinity estimation based damage localization approach in the context of automated structural health monitoring. In: 9th European Workshop on Structural Health Monitoring (EWSHM 2018); 2018.
10. Entezami A, Shariatmadar H. An unsupervised learning approach by novel damage indices in structural health monitoring for damage localization and quantification. *Struct Health Monit*. 2018;17(2):325-345. doi:10.1177/1475921717693572
11. Johnson EA, Lam HF, Katafygiotis LS, Beck JL. Phase i iasc-asce structural health monitoring benchmark problem using simulated data. *J Eng Mech*. 2004;130(1):3-15.
12. Dyke S, Bernal D, Beck J, Ventura C. Experimental phase ii of the structural health monitoring benchmark problem. In: Proceedings of the 16th ASCE Engineering Mechanics Conference; 2003:1-7.
13. Molina FJ, Pascual R, Golinval J-C. Description of the steelquake benchmark. *Mech Syst Sig Process*. 2003;17(1):77-82.
14. Antoniadou I, Dervilis N, Papatheou E, Maguire AE, Worden K. Aspects of structural health and condition monitoring of offshore wind turbines. *Phil Trans R Soc A: Math Phys Eng Sci*. 2015;373(2035):20140075. doi:10.1098/rsta.2014.0075
15. Ou Y, Chatzi EN, Dertimanis VK, Spiridonakos MD. Vibration-based experimental damage detection of a small-scale wind turbine blade. *Struct Health Monit*. 2017;16(1):79-96. doi:10.1177/1475921716663876
16. Tsiapoki S, Häckell MW, Grießmann T, Rolfes R. Damage and ice detection on wind turbine rotor blades using a three-tier modular structural health monitoring framework. *Struct Health Monit*. 2018;17(5):1289-1312.
17. Krause T, Ostermann J. Damage detection for wind turbine rotor blades using airborne sound. *Struct Control Health Monit*. 2020;27(5): e2520. e2520 stc.2520.
18. Tsiapoki S, Bahrami O, Häckell MW, Lynch JP, Rolfes R. Combination of damage feature decisions with adaptive boosting for improving the detection performance of a structural health monitoring framework: validation on an operating wind turbine. *Struct Health Monit*. 2021;20(2):637-660.
19. Penner N, Grießmann T, Rolfes R. Monitoring of suction bucket jackets for offshore wind turbines: Dynamic load bearing behaviour and modelling. *Marine Struct*. 2020;72:102745.
20. Ou Y, Tatsis KE, Dertimanis VK, Spiridonakos MD, Chatzi EN. Vibration-based monitoring of a small-scale wind turbine blade under varying climate conditions. part I: an experimental benchmark. *Struct Control Health Monit*. 2020:e2660. e2660 stc.2660.
21. Farrar CR, Cornwell PJ, Doebling SW, Prime MB. Structural health monitoring studies of the alamosa canyon and i-40 bridges. 2000. Los Alamos National Laboratories.
22. Maeck J, De Roeck G. Description of z24 benchmark. *Mech Syst Sig Process*. 2003;17(1):127-131.
23. Roeck GD. The state-of-the-art of damage detection by vibration monitoring: the simces experience. *J Struct Control*. 2003;10(2):127-134. doi:10.1002/stc.20
24. Peeters B, De Roeck G. One-year monitoring of the z24-bridge: environmental effects versus damage events. *Earthq Eng Struct Dyn*. 2001;30(2):149-171.
25. Yan A-M, Kerschen G, De Boe P, Golinval J-C. Structural damage diagnosis under varying environmental conditions-part ii: local pca for non-linear cases. *Mech Syst Sig Process*. 2005;19(4):865-880.
26. Reynders E, Roeck GD. Continuous vibration monitoring and progressive damage testing on the z24 bridge. *Encyclopedia of Structural Health Monitoring*: American Cancer Society; 2009.
27. Spiridonakos MD, Chatzi EN, Sudret B. Polynomial chaos expansion models for the monitoring of structures under operational variability. *ASCE-ASME J Risk Uncertain Eng Syst, Part A: Civil Eng*. 2016;2(3):B4016003.
28. Sarmadi H, Entezami A, Saeedi Razavi B, Yuen K-V. Ensemble learning-based structural health monitoring by mahalanobis distance metrics. *Struct Control Health Monit*. 2021;28(2):e2663. e2663 STC-20-0113.R1.
29. Andersen P, Brincker R, Peeters B, Roeck G, Hermans L, Krämer C. Comparison of system identification methods using ambient bridge test data. In: Proceedings of the 17th International Modal Analysis Conference (IMAC), Kissimmee, Florida, USA; 1999:1035-1041.
30. Brincker R, Andersen P, Cantieni R. Identification and level I damage detection of Z24 highway bridge. *Exper Tech*. 2001;25(6):51-57. doi:10.1111/j.1747-1567.2001.tb00047.x
31. Peeters B, Ventura CE. Comparative study of modal analysis techniques for bridge dynamic characteristics. *Mech Syst Sig Process*. 2003; 17(5):965-988.
32. Siringoringo DM, Fujino Y, Nagayama T, Wenzel H. Vibration characteristics of an overpass bridge during full-scale destructive testing. *Procedia Eng*. 2011;14:777-784. The Proceedings of the Twelfth East Asia-Pacific Conference on Structural Engineering and Construction.
33. Casas JR, Moughty JJ. Bridge damage detection based on vibration data: past and new developments. *Front Built Environ*. 2017;3:4.

34. Döhler M, Hille F, Mevel L, Rücker W. Structural health monitoring with statistical methods during progressive damage test of s101 bridge. *Eng Struct*. 2014;69:183-193.
35. Giordano PF, Limongelli MP. Vibration-based damage identification for the s101 benchmark bridge: a comparison of indicators. In: 9th European Workshop on Structural Health Monitoring (EWSHM 2018); 2018.
36. Fathi A, Limongelli MP. Statistical vibration-based damage localization for the s101 bridge, flyover reibersdorf, austria. *Struct Infrastruct Eng*. 2020;0(0):1-15.
37. Li S, Li H, Liu Y, Lan C, Zhou W, Ou J. Smc structural health monitoring benchmark problem using monitored data from an actual cable-stayed bridge. *Struct Control Health Monit*. 2014;21(2):156-172. doi:10.1002/stc.1559
38. Huang J, Li D, Li H, Song G, Liang Y. Damage identification of a large cable-stayed bridge with novel cointegrated kalman filter method under changing environments. *Struct Control Health Monit*. 2018;25(5):e2152. e2152 STC-17-0200.R1.
39. Steenackers G, Guillaume P. Structural health monitoring of the z-24 bridge in presence of environmental changes using modal analysis. In: Conference Proceedings of International Modal Analysis Conference (IMAC23); 2005.
40. Institute of Meteorology and Climatology. Current Measurements of Hannover Herrenhausen and Ruthe. Accessed April 16, 2021. https://www.muk.uni-hannover.de/258.html?&L=1
41. Häckell MW, Rolfes R, Kane MB, Lynch JP. Three-tier modular structural health monitoring framework using environmental and operational condition clustering for data normalization: Validation on an operational wind turbine system. *Proc IEEE*. 2016;104(8):1632-1646.
42. Peeters B, De Roeck G. Stochastic subspace system identification of a steel transmitter mast. *IMAC 16, the Int Modal Anal Confer*. 1998;3243:130-136.
43. Reynders E, Pintelon R, De Roeck G. Uncertainty bounds on modal parameters obtained from stochastic subspace identification. *Mech Syst Sig Process*. 2008;22(4):948-969. Special Issue: Crack Effects in Rotordynamics.
44. Katayama T. *Subspace Methods for System Identification*, Communications and Control Engineering. London: Springer; 2006.
45. van Overschee P, de Moor BL. *Subspace Identification for Linear Systems: Theory—Implementation—Applications*. US: Springer; 2012.
46. Reynders E, Houbrechts J, De Roeck G. Fully automated (operational) modal analysis. *Mech Syst Sig Process*. 2012;29:228-250.
47. Welch P. The use of fast fourier transform for the estimation of power spectra: a method based on time averaging over short, modified periodograms. *IEEE Trans Audio Electroacoustics*. 1967;15(2):70-73.
48. Brincker R, Ventura C. *Introduction to Operational Modal Analysis*. New York: John Wiley & Sons; 2015.
49. Allemang R. The modal assurance criterion (MAC): twenty years of use and abuse. *Sound Vib*. 2003;37:14-23.
50. Tamura Y, Suganuma S. Evaluation of amplitude-dependent damping and natural frequency of buildings during strong winds. *J Wind Eng Ind Aerodyn*. 1996;59(2):115-130.
51. Ma J. Estimation of amplitude-dependent dynamic parameters from ambient vibration data. *In Advances in Environmental Vibration and Transportation Geodynamics*. Singapore: Springer; 2020:679-689. doi:10.1007/978-981-15-2349-6_43
52. Norén-Cosgriff K, Kaynia AM. Estimation of natural frequencies and damping using dynamic field data from an offshore wind turbine. *Marine Struct*. 2021;76:102915. doi:10.1016/j.marstruc.2020.102915
53. Tamura Y. Amplitude dependency of damping in buildings and critical tip drift ratio. *Int J High-Rise Build*. 2012;1:1-13.
54. Yang B, Zhu H, Wüchner R, Zhang Q. Monitoring of wind effects on a wind-sensitive hybrid structure with single-layer cable-net curtain walls under typhoon muifa. *J Build Eng*. 2021;44:102960. doi:10.1016/j.jobe.2021.102960
55. Worden K, Tomlinson GR. *Nonlinearity in Structural Dynamics—Detection, Identification and Modelling*: Institute of Physics Publishing; 2019.
56. Peeters B, Maeck J, Roeck GD. Vibration-based damage detection in civil engineering: excitation sources and temperature effects. *Smart Mater Struct*. 2001;10(3):518-527.
57. Koo KY, Brownjohn JMW, List DI, Cole R. Structural health monitoring of the tamar suspension bridge. *Struct Control Health Monit*. 2013;20(4):609-625. doi:10.1002/stc.1481
58. Martín-Sanz H, Tatsis K, Dertimanis VK, Avendaño-Valencia LD, Brühwiler E, Chatzi E. Monitoring of the UHPFRC strengthened Chillon viaduct under environmental and operational variability. *Struct Infrastruct Eng*. 2020;16(1):138-168.
59. Rainieri C, Fabbrocino G. *Operational Modal Analysis of Civil Engineering Structures—An Introduction and Guide for Applications*. Berlin, Heidelberg: Springer; 2014.
60. Au S-K, Zhang F-L, Ni Y-C. Bayesian operational modal analysis: theory, computation, practice. *Computers & Structures*. 2013;126:3-14. doi:10.1016/j.compstruc.2012.12.015
61. Au S-K. *Operational Modal Analysis—Modeling, Bayesian Inference, Uncertainty Laws*: Springer Singapore; 2017. doi:10.1007/978-981-10-4118-1
62. Au S-K, Brownjohn JMW, Li B, Raby A. Understanding and managing identification uncertainty of close modes in operational modal analysis. *Mech Syst Sig Process*. 2021;147:107018.
63. Brincker R, Lopez-Aenlle M. Mode shape sensitivity of two closely spaced eigenvalues. *J Sound Vib*. 2015;334:377-387.
64. D'Ambrogio W, Fregolent A. Higher-order mac for the correlation of close and multiple modes. *Mech Syst Sig Process*. 2003;17(3):599-610.
65. Zhang L, Brincker R, Andersen P. Modal indicators for operational modal identification. In: Proceedings of IMAC 19; 2001:746-752.
66. Avendaño-Valencia LD, Chatzi EN, Koo KY, Brownjohn JMW. Gaussian process time-series models for structures under operational variability. *Frontiers in Built Environment*. 2017;3:69.

67. Dodge Y. *The Concise Encyclopedia of Statistics*. New York: Springer; 2010.
68. Jolliffe IT. *Principal Component Analysis*: Springer; 2002. doi:10.1007/b98835
69. Gardner P, Bull LA, Dervilis N, Worden K. Overcoming the problem of repair in structural health monitoring: Metric-informed transfer learning. *J Sound Vib*. 2021;510:116245. doi:10.1016/j.jsv.2021.116245

How to cite this article: Wernitz S, Hofmeister B, Jonscher C, Grießmann T, Rolfes R. A new open-database benchmark structure for vibration-based Structural Health Monitoring. *Struct Control Health Monit*. 2022;29(11): e3077. doi:10.1002/stc.3077